An Assessment of the Applicability of Multifrequency ESR to Study the Complex Dynamics of Biomolecules

Zhichun Liang and Jack H. Freed*

Baker Laboratory of Chemistry and Chemical Biology, Cornell University, Ithaca, New York 14853-1301

Received: March 4, 1999; In Final Form: May 17, 1999

It is shown that the commonly used models for analyzing ESR spectra from nitroxide spin-labeled proteins or DNA systems are special cases of the more general slowly relaxing local structure (SRLS) model, wherein the nitroxide spin probe is taken as reorienting in a restricted local environment, which itself is relaxing on a longer time scale. This faster motion describes the internal dynamics, while the slower motion describes the global tumbling of the macromolecule. By using the SRLS model as the reference, it is shown (1) under what conditions the microscopic-order macroscopic-disorder (MOMD) model, wherein the global tumbling of the macromolecule is in the rigid limit, is valid, and (2) when the fast internal motion (FIM) model, wherein the internal motion is so rapid as to lead to partial averaging of the magnetic tensors, is valid. The frequency dependence of these models is studied. A key general property of high frequency ESR that emerges is that it reports on a faster motional time scale, whereas low frequency ESR reports on a slower motional time scale. It is shown that, in general, the MOMD model is a better approximation for ESR spectra obtained at high frequency (250 GHz), whereas, in general, the FIM model is a better approximation for low frequency (9 GHz) ESR spectra. However, in general, one does not find that the simpler model fits, at a single ESR frequency, to the more complete SRLS model, return correct motional and ordering parameters. The simultaneous fitting of both low and high frequency ESR spectra is thus required to remove such ambiguities and to return all the various dynamic, ordering, and geometric factors that characterize the complex dynamics. This approach is briefly related to recent ESR spectra from the spin-labeled protein, T4 lysozyme, and from spin-labeled DNA nucleosides. In order to better apply the slow-motional SRLS model to macromolecular dynamics, the Polimeno−Freed theory has been extended to the case where the global tumbling is anisotropic and where the angle between the principal axis of the global motion and the preferred orientation of the internal modes of motion is arbitrary.

1. Introduction

Ever since the advent of nitroxide spin labeling, it has been clear that ESR studies of spin-labeled macromolecules can provide insight into their complex dynamics.[1] The recent development of the method of site directed spin-labeling of proteins[2] opens the potential to examine the local dynamical modes at or near each labeled residue (plus the overall motions) thereby ultimately leading to a "map" of the dynamic structure throughout the protein or other macromolecule. In addition, the development of modern ESR methods with enhanced sensitivity to reorientational dynamics such as two-dimensional Fourier transform ESR[3,4] and high field/high frequency ESR,[5,6] may be expected to improve one's ability to unravel the complex dynamic modes from ESR spectroscopy.

In this paper, we wish to examine how a multifrequency approach, using high as well as low (or standard) ESR frequencies (but otherwise conventional cw methods), can usefully address the decomposition of the complex dynamic modes affecting each site label. This primarily theoretical analysis is motivated, at least in part, by encouraging initial results on site-directed spin-labeled protein: T4-lysozyme using ESR spectra at 9 and 250 GHz.[7] In addition, recent studies on spin-labeled DNA nucleosides are encouraging in studying DNA dynamics.[8]

Let us first analyze the various motions existing in a spin-labeled protein system (cf. Figure 1). These motions may be roughly classified into three groups. (i) First, the globular protein may undergo an overall isotropic tumbling. (ii) Specific side chains within the protein may also fluctuate around an average orientation. (iii) Finally, the spin labels reorient rapidly with respect to the alkyl side chains. Detailed discussions of the various motions in proteins include recent reviews by Kay[9] and Peng and Wagner.[10]

The rotational motions existing in a spin-labeled DNA system may also be grouped in a similar manner[11,12] (cf. Figure 2). (i) The first motion is the global tumbling of the whole DNA helix. (ii) The second group consists of collective uniform bending and twisting motions of base pairs. (iii) The next group is the motion of an individual base which also includes the twisting and bending modes. For example, a base pair may undergo a large amplitude opening and closing reaction and a small amplitude libration. (iv) Finally the spin-label reporter group may experience a local reorientation with respect to the bond which connects the nitroxide moiety and the base.

In principle, a complete dynamical model should include all of these motions. However, a useful model may only explicitly describe a few "composite" modes of motion, because of the computational limitations as well as the limited experimental resolution available. A common practice when investigating the dynamic behavior of protein and DNA systems is to separate

* Corresponding author. E-mail: jhf@msc.cornell.edu. Fax: (607) 255-0595.

10.1021/jp9907746 CCC: $18.00
Published on Web 07/29/1999

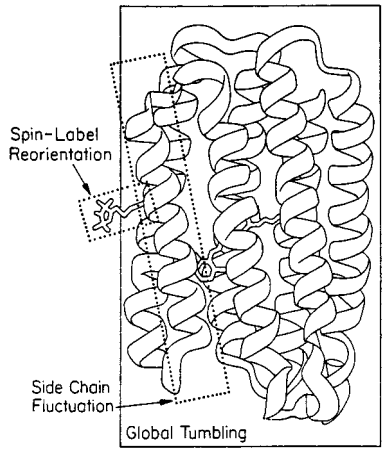

Figure 1. Schematic illustration of the various dynamical processes in a protein system. It is adapted from Figure 1 in ref 17.

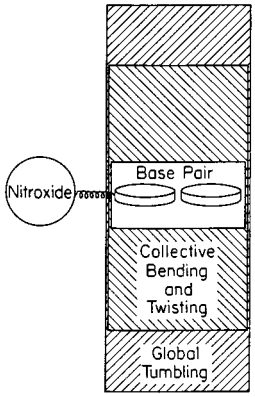

Figure 2. Schematic illustration of the various dynamical processes in a DNA system. It is adapted from Figure 1 in ref 47.

the global tumbling from the other motions. In this approach, one first views the dynamics in the lab frame, observing the overall reorientation of, for example, a globular protein or a DNA helix, which is assumed to be a freely diffusing rigid sphere or cylinder, respectively. We then jump to a reference frame, which is rigidly attached to the sphere or cylinder, to observe the other motions. In other words, the effects of these motions are combined and the resultant dynamics is referred to as the internal motion. While the overall motion of the proteins or DNA can be estimated from hydrodynamic theory, the internal motion is less well characterized. However, the internal motion is of general interest in connection with many biological processes such as dye intercalation, enzyme reactions, and protein−DNA interactions.[11,12]

Nuclear magnetic resonance (NMR) has been an important technique for probing the rotational dynamics in macromolecules. A variety of models for internal motion was formulated by Lipari and Szabo[13] to extract dynamic information from NMR relaxation studies of deoxyribonucleic acid fragments. However, it was found that the data they used seemed too limited to lead to a unique physical picture of internal motions in DNA fragments. They later developed a "model free" approach[14] which has been widely used to interpret NMR relaxation in macromolecules.[15] A generalized order parameter and an effective correlation time can be specified for internal motion from relaxation experiments.

As we discussed above, ESR is another powerful tool for studying the dynamic processes in macromolecules such as protein[16−20] and DNA[21−25] systems. Because of its favorable time scale, ESR experiments can be even more sensitive to the details of the rotational dynamics in these systems. That is, ESR involves orientation-dependent terms in the spin-Hamiltonian (in units of frequency) which are at much higher freqency than is the case for such NMR terms. Thus, in NMR the (complex) molecular dynamics leads to nearly complete averaging of the orientation-dependent terms in liquids with their residual effects nearly always reflected only in the relaxation times T_1 and T_2, which may be calculated by a second-order perturbation theory commonly referred to as Redfield theory.[26] However, given the much larger magnitude of the ESR terms, the effects of the orientation-dependent terms are often more dramatic and cannot be analyzed by a perturbational approach. In order to extract useful dynamic information from such ESR experiments, a slow motional theory based on the stochastic Liouville equation (SLE) has been developed,[27−31] which shows that the more dramatic lineshape changes are particularly sensitive to microscopic details of the dynamics. Furthermore, as one increases the magnetic field and frequency in ESR, the role of the **g**-tensor in the spin-Hamiltonian grows linearly. Thus, at high fields and frequencies, the breakdown of perturbative relaxation theories becomes more dramatic, so the SLE is required over a greater range of motional rates.[32]

Even more important than this is the simple fact that ESR at higher frequencies will be more sensitive to the faster dynamics but will lose its sensitivity to the slower dynamics, as compared to ESR at the lower freqencies. We may speak of the "time scale" of high frequency ESR being faster than that of low frequency ESR. Thus, for example, the faster internal dynamic modes of a macromolecule may be so fast on the slower time scale of low frequency ESR that one just observes the spectrum wherein these motions are completely averaged out, whereas on the faster time scale of high frequency ESR their effects are clearly discernable. On the other hand, the overall tumbling of the macromolecule may be so slow on the fast time scale of high frequency ESR that it is completely frozen out, whereas on a slower time scale it is substantially affects the ESR spectrum. In this paper we will clearly illustrate these matters.

The slow motional ESR theory was recently extended to explicitly account for coupled dynamical motions occuring at different time scales.[33] In the slowly relaxing local structure (SRLS) model,[34,35] the spin probe is assumed to be reorienting in a local environment which itself is relaxing on a longer time scale. When applied to macromolecular systems, the faster motion of the SRLS model is used to describe the internal dynamics, while the slower motion accounts for the global rotation of the macromolecule.

We wish to note here that the SRLS model, which was first used in ESR by Polnaszek and Freed[34] and in NMR by Freed[35] in the context of liquid-crystal dynamics, largely in the motionally narrowed regime, by Campbell et al.,[36] is a quite general one with many possible applications. Since high frequency ESR is almost always in the slow motional regime, the extension of SRLS to the slow motional regime by means of the SLE was important.[33,37] In the fast motional regime, it should be mentioned that the "model free" approach of Lipari and Szabo[14,15] has many features that are similar to the SRLS model. A detailed theoretical analysis of the SRLS model has been reviewed by Polimeno and Freed.[38]

In nearly all previous ESR studies, the physical picture was even further simplified. First it was assumed that the global and the internal motions occur at different time scales, so that their dynamic effects can be separated. In addition, it was assumed that either the internal motion is in the very fast motional limit, or else the global motion is in the rigid limit, so

that only one type of dynamic process is evident in the spectrum and/or the relaxation behavior. In the fast internal motion (FIM) models,[39,40] the internal dynamics, which leads to partial averaging of the magnetic tensors, is characterized by an "effective" order parameter, and the global motion is described in terms of diffusion constant(s). In the model in which the overall motion is frozen out, the internal dynamics is specified in terms of the preferred orientation of the internal motion and the orientational potentials about the preferred orientation, yielding local order parameters and the rotational diffusion tensor for the internal motion. This model is usually referred to as the MOMD model, i.e., microscopic order but macroscopic disorder.[41,42] The very early simplified model of McConnell and co-workers,[43,44] which may be referred to as an "averaged Hamiltonian" model, is in fact the limit when both FIM and MOMD models are valid, i.e., frozen overall motion and (nearly) complete averaging over the internal modes.

In our present study we make use of the more sophisticated SRLS model with special emphasis on its applications to protein and DNA systems. Utilizing this SRLS model we are also able to discuss the range of validity of the FIM and MOMD limiting models.

The paper is organized as follows. In section 2, we present the theoretical basis of the latest version of the SRLS model in the context of slow motional theory, that is particularly applicable for complex macromolecular dynamics. In the original SRLS treatment by Polimeno and Freed,[33] the diffusing body for the slower motion is assumed to be of spherical shape. Since macromolecules may often be better approximated by other shapes (e.g., cylinders), the SLRS model is extended in this paper to model the overall motion of the macromolecule by anisotropic rotational diffusion. This further requires that one specify the tilt between the principal axes of overall diffusion and the preferred orientation of the internal modes of motion within the macromolecule. In section 3, we discuss the various models for the internal dynamics which are of biological interest. We then show under which conditions the limiting motional models in the literature can be derived from our general model in section 4. In section 5, we present some ESR spectral simulations to establish the range of validity of the simplified models and to consider the efficacy of the multifrequency approach. Finally in section 6, the main conclusions are summarized along with some additional comments.

2. Anisotropic SRLS Model

We will now describe the anisotropic SRLS (or cage) model, which treats explicitly both the internal motion and the global tumbling. Let us first define a few coordinate systems, (cf. Figure 3). The laboratory frame (LF) is a frame at rest whose *z*-axis is parallel to the applied magnetic field B_0. Then to describe the global tumbling, we define a global diffusion frame, with its *z*-axis taken along a principal axis of the macromolecule, e.g., the long axis of the cylinder for a DNA molecule or a rodlike protein. This frame will be called the cage frame and is denoted as CF.[33] The Euler angles Ω_{LC}, which transform the C frame to the lab frame, are modulated by the global tumbling of the macromolecule, i.e., the instantaneous orientation of the macromolecule relative to the lab frame, is specified by Ω_{LC}. In a similar manner, to model the internal motion, we define an internal diffusion frame, MF, which is defined as the symmetry axes for the diffusion of the internal modes of motion. Then the Euler angles relating the MF and the LF Ω_{LM} are modulated by both the internal dynamics and the overall tumbling. Now our discussion will be restricted to isotropic

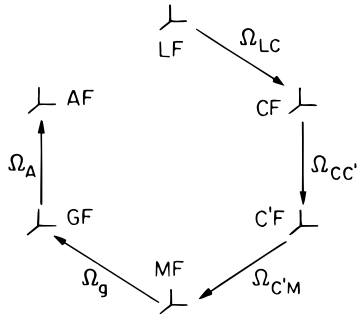

Figure 3. Reference frames which define the structural and dynamic properties of the combined system of spin-labeled moiety and macromolecule. LF = lab frame, CF = cage frame, C′F = internal director frame, MF = internal diffusion frame, GF = *g* tensor frame, AF = *A* tensor frame.

solutions, (not necessary, but sufficient for present purposes), so that the macromolecule reorients in an isotropic medium. However, the internal motion will experience a mean orienting potential with symmetry axes that may be tilted relative to the CF. We therefore define an internal ordering frame, C′F, also known as the internal director frame, or the tilt cage frame, because it is a frame fixed in the macromolecule. This frame may be tilted from the CF by Euler angles $\Omega_{CC'} = (0, \beta_{CC'}, 0)$ assumed to be time independent. Note that, for simplicity, we take the MF to be the principal axes both for diffusion and for orientational restriction of the internal modes of motion. Finally the internal diffusion frame may be tilted from the magnetic **g**-tensor frame (assumed to coincide with magnetic **A**-tensor frame) GF by static Euler angles $\Omega_{MG} = (\alpha_{MG}, \beta_{MG}, \gamma_{MG})$.

To complete defining the anisotropic cage model, we next write down the time dependent part of the spin Hamiltonian for this two body system:[33]

$$\hat{H} = \sum_{\mu=g,A}\sum_{l=0,2}\sum_{m=-l}^{l}\sum_{m'=-l}^{l}\sum_{m''=-l}^{l}\hat{A}^{(l,m)}_{\mu,L} D^{l}_{mm'}(\Omega_{LM}) D^{l}_{m'm''}(\Omega_{MG}) F^{(l,m'')*}_{\mu,G} \quad (1)$$

where $X^{(l,m)}_{\mu,N}$ stands for the *m*th component of the *l*th rank irreducible spherical tensor or tensor operator *X* defined in the N frame, with μ specifying the kind of interaction [Zeeman (*g*) or hyperfine (*A*)]: $D^{l}_{nn'}(\Omega_{NN'})$'s are Wigner rotation matrix elements which relate the N frame to the N′ frame. The detailed form of $\hat{A}^{(l,m)}_{\mu,L}$ and $F^{(l,m'')}_{\mu,G}$ can be found elsewhere.[30] It can be seen from eq 1 that the spin Hamiltonian depends on the modulation of Ω_{LM} due to both types of motion. The dynamic effects of both the global tumbling and the internal motions are incorporated into the ESR line shape through the diffusion operator

$$\hat{\Gamma} = \hat{\Gamma}^{global}(\Omega_{LC}) + \hat{\Gamma}^{internal}(\Omega_{LM}) + F^{global}(-\Omega_{C'M}) + F^{internal}(-\Omega_{C'M}) \quad (2)$$

The first two terms in this equation refer respectively to the isotropic portions of the two motions, which are functions of the respective Euler angles. The last two terms are the contributions due to the internal orienting potential, which couples the internal and global tumbling motions. They are thus a function of $\Omega_{C'M}$, which transforms the MF into the C′F. It can be further expressed as the overall effect of the successive rotations: $-\Omega_{CC'} - \Omega_{LC} + \Omega_{LM}$.

When modeling the global tumbling, we usually consider the protein or DNA fragment as either spherical or a rigid cylinder,

which undergoes free Brownian diffusion. That is, we adopt a rotational diffusion expression that assumes axial symmetry for convenience. (This simplifying assumption is, of course, not necessary, cf. ref 33). That is

$$\hat{\Gamma}^{\text{global}}(\Omega_{\text{LC}}) = R_{\perp}^{\text{c}}\hat{\mathbf{J}}^{\text{c}2} + (R_{\parallel}^{\text{c}} - R_{\perp}^{\text{c}})\hat{\mathbf{J}}_z^{\text{c}2} \quad (3)$$

Here $\hat{\mathbf{J}}^{\text{c}}$ is equal to the vector operator that generates an infinitesimal rotation of the probe (except for a factor $-i$), with components specified in the CF. Thus, the global motion is completely specified by two diffusion constants, $R_{\perp}^{\text{c}}$ and $R_{\parallel}^{\text{c}}$, describing the wobbling and spinning motions of the "cylinder", respectively. To a first approximation, these constants can be estimated from the approximate hydrodynamic expressions.[45]

By contrast, the internal motion is more complex in nature. As we may recall from the introduction, the internal motion consists of the collective and individual base motions for DNA, or the side-chain fluctuations for a protein, as well as the spin-label motion in both cases. In a particular experiment, one or several modes of these motions may be monitored, and for different modes, different models may need to be employed. A few models have been developed in several studies on the internal motions of DNA and of proteins, and some of them will be mentioned below.

In most cases, the internal motion is modeled as an anisotropic Brownian diffusion[30,42]

$$\hat{\Gamma}^{\text{internal}}(\Omega_{\text{LM}}) = \hat{\mathbf{J}}^{\text{o}}\cdot R^{\text{o}}\cdot\hat{\mathbf{J}}^{\text{o}} \quad (4)$$

where $\hat{\mathbf{J}}^{\text{o}}$ is the infinitesimal rotation operator for the internal motion, and the rotational diffusion tensor for this motion has principal components R_{xx}^{o}, R_{yy}^{o} and R_{zz}^{o}. In the special case that $R_{xx}^{\text{o}} = R_{yy}^{\text{o}} = R_{\perp}^{\text{o}}$ and $R_{zz}^{\text{o}} = R_{\parallel}^{\text{o}}$, eq 4 becomes

$$\hat{\Gamma}^{\text{internal}}(\Omega_{\text{LM}}) = R_{\perp}^{\text{o}}\hat{\mathbf{J}}^{\text{o}2} + (R_{\parallel}^{\text{o}} - R_{\perp}^{\text{o}})\hat{\mathbf{J}}_z^{\text{o}2} \quad (5)$$

Now the internal motion within the macromolecule (cage) is restricted, and this is represented by an orienting potential, $U(\Omega_{C'\text{M}})$, which is assumed to take the following form

$$U(\Omega_{C'\text{M}})/k_{\text{b}}T = c_0^2\, D_{00}^2(\Omega_{C'\text{M}}) + c_2^2[D_{02}^2(\Omega_{C'\text{M}}) + D_{0-2}^2(\Omega_{C'\text{M}})] \equiv u(\Omega_{C'\text{M}}) \quad (6)$$

i.e., this represents internal motion relative to the preferred orientation in the cage given by C′F. More generally we can expand $U(\Omega_{C'\text{M}})$ in a complete set of $D_{K,M}^{L}(\Omega_{C'\text{M}})$, but eq 6 is the simplest form consistent with the model.[33] This will lead to a set of operator expressions for F^{internal} and F^{global} which appear in the complete diffusion operator given by eq 2:

$$F^{\text{internal}} = \frac{1}{2}(R_{\perp}^{\text{o}}(\hat{\mathbf{J}}^{\text{o}2}u) + (R_{\parallel}^{\text{o}} - R_{\perp}^{\text{o}})(\hat{\mathbf{J}}_z^{\text{o}2}u)] - \frac{1}{4}[(R_{\perp}^{\text{o}})(\hat{\mathbf{J}}_{+}^{\text{o}}u)(\hat{\mathbf{J}}_{-}^{\text{o}}u) + R_{\parallel}^{\text{o}}(\hat{\mathbf{J}}_z^{\text{o}}u)^2] \quad (7)$$

and

$$F^{\text{global}} = \frac{1}{2}(R_{\perp}^{\text{c}}(\hat{\mathbf{J}}^{\text{c}2}u) + (R_{\parallel}^{\text{c}} - R_{\perp}^{\text{c}})(\hat{\mathbf{J}}_z^{\text{c}2}u)] - \frac{1}{4}[(R_{\perp}^{\text{c}})(\hat{\mathbf{J}}_{+}^{\text{c}}u)(\hat{\mathbf{J}}_{-}^{\text{c}}u) + R_{\parallel}^{\text{c}}(\hat{\mathbf{J}}_z^{\text{c}}u)^2] \quad (8)$$

We therefore have four model parameters in the simplest case for the internal motion: two diffusion constants describing diffusion parallel and perpendicular to the principal internal diffusion axis, $R_{\perp}^{\text{o}}$ and $R_{\parallel}^{\text{o}}$, respectively, as well as two potential coefficients c_0^2 and c_2^2. (Note that $c_2^2 \neq 0$ if the orienting potential is asymmetric about the internal ordering axis). When applied to protein systems, these model parameters describe the side-chain reorientation. In the case of DNA, it is reasonable to assume that the collective base motion is slower than the individual base motions, since the former involves collective movement of more than one base. So if the individual motion is observed and the collective motion is in the rigid limit, then these parameters describe the individual motion and the effect of the collective motion can be included in the Euler angle $\Omega_{CC'}$. On the other hand, if the collective motion is monitored and the individual motion is in the fast limit, then the internal motion model describes the collective motion and the effect of the individual motion can be accounted for by the Euler angle Ω_{MG}.

Now we would like to summarize the model parameters of the anisotropic cage model in its simplest useful form. They are four diffusion constants, $R_{\perp}^{\text{o}}$, $R_{\parallel}^{\text{o}}$, $R_{\perp}^{\text{c}}$, and $R_{\parallel}^{\text{c}}$, two potential parameters, c_0^2 and c_2^2, and two polar angles $\beta_{CC'}$ (cage tilt) and β_{MG} (diffusion tilt).

3. Simplified Models at Different Motional Limits

From the above discussion, it is clear that there are at least eight model parameters in the anisotropic cage model, if the anisotropic diffusion model is used for the overall motion. Furthermore, the total number of fitting parameters will become 14 when two sites are required to calculate a spectrum (cf. section 5), since each site will have its own internal dynamics. However, the experimental data measured under normal conditions are usually too limited to uniquely determine these parameters. One way of overcoming this problem would be to obtain more extensive data at different magnetic fields and frequencies, a matter we shall turn to in the next section. However, in the past, simplified models have been introduced to reduce the number of parameters to be fit. We consider the main ones below and show that they are special limiting cases of the SRLS model.

3.1. Very Slow Gobal Tumbling: MOMD Model. For a relatively long DNA or large protein aggregate, the global rotation of the whole body may become too slow to be observed in an ESR experiment. As a result, we will see a static uniform orientational distribution of the cylinders, so that the Euler angles $\Omega_{LC'} = \Omega_{\text{LC}} + \Omega_{CC'}$, become time independent. Thus, the internal motion can be defined with respect to the internal ordering frame C', which is now fixed in the lab frame for each local site in the sample. Thus

$$\hat{H} = \sum_{\mu=g,A}\sum_{l=0,2}\sum_{m=-l}^{l}\sum_{m'=-l}^{l}\sum_{m''=-l}^{l}\sum_{m'''=-l}^{l}\hat{A}_{\mu,L}^{(l,m)} D_{mm'}^{l}(\Omega_{LC'})D_{m'm''}^{l}(\Omega_{C'\text{M}})D_{m''m'''}^{l}(\Omega_{\text{MG}})F_{\mu,\text{G}}^{(l,m''')*} \quad (9)$$

This Hamiltonian defines the MOMD model (cf. section I) for which the internal diffusion axis is microscopically ordered within each macromolecule but the internal ordering axis for each macromolecule in the sample is macroscopically disordered, i.e., randomly oriented in space. Now only the internal motion contributes to the diffusion operator.[41]

$$\hat{\Gamma} = \hat{\Gamma}^{\text{internal}}(\Omega_{C'\text{M}}) + F^{\text{internal}}(\Omega_{C'\text{M}}) \quad (10)$$

The parameter space of this model contains only the following five parameters for the internal motion, $R_{\perp}^{\text{o}}$, $R_{\parallel}^{\text{o}}$, c_0^2, c_2^2, and β_{MG}.

3.2. Very Fast Internal Motion: FIM Model. We next consider another motional limit, where the internal motion is in the extreme narrowing regime, i.e., the FIM model (cf. section 1). In this limit, we cannot observe the dynamic effect of the internal motion but only its averaging effect. This enables us to perform an ensemble average of the spin Hamiltonian over the internal variables. If we further assume that the internal and the overall motions occur at different time scales, then, in a time interval, τ, which is short compared with the global tumbling time scale but long compared with the internal motional time scale, i.e.,

$$\tau_{\text{global}} \gg \tau \gg \tau_{\text{internal}} \tag{11}$$

the slower motion will appear static. In this case, an average can be performed on the rotational transformation matrix elements $D^2_{m''m'''}(\Omega_{C'M})$, which gives one or a few time independent order parameters. The spin Hamiltonian for the FIM model is then given by

$$\hat{H} = \sum_{\mu=g,A}\sum_{l=0,2}\sum_{m=-l}^{l}\sum_{m'=-l}^{l}\sum_{m''=-l}^{l}\sum_{m'''=-l}^{l}\sum_{m''''=-l}^{l}\hat{A}^{(l,m)}_{\mu,\text{L}} D^{l}_{mm'}(\Omega_{\text{LC}})D^{l}_{m'm''}(\Omega_{\text{CC}'})\langle D^{l}_{m''m'''}(\Omega_{C'M})\rangle D^{l}_{m'''m''''}(\Omega_{\text{MG}})F^{(l,m'''')*}_{\mu,\text{M}} \tag{12}$$

where the angular brackets indicate ensemble averaged quantities, (cf. below).

The number of the order parameters, $\langle D^2_{m''m'''}(\Omega_{C'M})\rangle$ (there are 25 of them in general) may be reduced by utilizing the symmetries of the system. If there is at least a 3-fold symmetry around the local director of the internal motion, i.e., C′F, then $m'' = 0$; and if there is at least a two-fold symmetry around the internal diffusion axis, then m''' is either 0 or ± 2. We then have $\langle D^2_{m''m'''}(\Omega_{C'M})\rangle = 0$ unless $m'' = 0$ and $m''' = 0$ or ± 2. If, in addition, only the polar angle β_{MG} is needed to transform between the M and G frames, $F^{(l,m'''')}_{\mu,\text{G}}$ will then depend on $|m''''|$. Then, one would only need to define two order parameters,

$$S^2_0 = \langle D^2_{00}[\Omega_{C'M}(t)]\rangle \tag{13}$$

$$S^2_2 = \langle D^2_{02}[\Omega_{C'M}(t)]\rangle + \langle D^2_{0-2}[\Omega_{C'M}(t)]\rangle \tag{14}$$

where the ensemble averages are defined in terms of the orienting potential in eq 6,

$$\langle D^2_{0n}[\Omega_{C'M}(t)]\rangle = \frac{\int d\Omega D^2_{0n}(\Omega)\exp[c_0^2 D^2_{00}(\Omega) + \text{H}2c_2^2 Re D^2_{02}(\Omega)]}{\int d\Omega \exp[c_0^2 D^2_{00}(\Omega) + \text{H}2c_2^2 Re D^2_{02}(\Omega)]} \tag{15}$$

The internal motion would be completely specified by these order parameters, S^2_0 and S^2_2. The diffusion operator is only dependent on the global dynamics, which is described by $R^c_\perp$ and $R^c_{||}$ [cf. eq 3]:

$$\hat{\Gamma} = \hat{\Gamma}^{\text{global}}(\Omega_{\text{LC}}) \tag{16}$$

The other parameters for the FIM model are $\beta_{\text{CC}'}$ and β_{MG}.

In a model developed by Timofeev and co-workers for protein systems,[40] the internal motion is also accounted for by two-order parameters. However, their global motion is described by only one diffusion constant, which implies that the protein complex is approximated as an isotropic body. This model can be obtained from our FIM model by setting the two global diffusion constants equal to each other. In a closely related dynamic model developed by Hustedt et al. for DNA systems,[39] two diffusion constants are explicitly included for the global motion, but the fast internal motion is characterized by a simple parameter, which is a measure of the total mean-squared amplitude of all internal motions. This parameter can be related to the order parameter S^2_0 defined in eq 14 when the the internal motion has a small amplitude of oscillation. Thus, this model is equivalent to our FIM model at high orienting potential. The dynamic cylinder model used by Keyes and co-workers[47] is another variant of our FIM model. However, instead of the order parameters, the magnetic **g** and **A** tensor components are varied in a spectral simulation. The order parameter is finally calculated from these tensor components.

3.3. FIM + Very Slow Wobbling Global Motion. For the case of DNA, the FIM model can be simplified by the fact that the length of a DNA helix is usually much larger than its diameter. As a result, when the spinning motion of the cylinder is in the slow motional region, the wobbling diffusion may be well into the rigid limit. If we explicitly express the Wigner rotation matrix for the global motion, we obtain the following spin Hamiltonian

$$\hat{H} = \sum_{\mu=g,A}\sum_{l=0,2}\sum_{m=-l}^{l}\sum_{m'=-l}^{l}\sum_{m''=-l}^{l}\sum_{m'''=-l}^{l}\hat{A}^{(l,m)}_{\mu,\text{L}} d^{l}_{mm'}(\beta_{\text{LC}})exp(-m'\gamma_{\text{LC}})D^{l}_{m'0}(\Omega_{\text{CC}'})S^2_{m''} D^{l}_{m''m'''}(\Omega_{\text{MG}})F^{(l,m''')*}_{\mu,\text{G}} \tag{17}$$

Here the polar angle β_{LC}, is now time independent, and a static averaging should be performed on it. On the other hand, the azimuthal angle γ_{LC} is modulated by the spinning motion, and its time evolution is governed by a new diffusion operator

$$\hat{\Gamma} = R^c_{||}\,\hat{\mathbf{J}}^{c2}_z \tag{18}$$

We are then left with five model parameters: $R^c_{||}$, S^2_0, S^2_2, $\beta_{\text{CC}'}$ and β_{MG}.

3.4. The Averaged Hamiltonian Model: MOMD + FIM. In this early model of McConnell and co-workers (cf. section 1) the global motion is assumed to be so slow that it is in the rigid limit, whereas the internal motion is so fast that it simply leads to partial averaging of the spin Hamiltonian. That is, we obtain the following time independent spin-Hamiltonian:

$$\hat{H} = \sum_{\mu=g,A}\sum_{l=0,2}\sum_{m=-l}^{l}\sum_{m'=-l}^{l}\sum_{m''=-l}^{l}\sum_{m'''=-l}^{l}\hat{A}^{(l,m)}_{\mu,\text{L}} D^{l}_{mm'}(\Omega_{\text{LC}'})\langle D^{l}_{m'm''}(\Omega_{C'M})\rangle D^{l}_{m''m'''}(\Omega_{\text{MG}})F^{(l,m''')*}_{\mu,\text{G}} \tag{19}$$

Thus only the order parameters S^2_0 and S^2_2 need to be specified, and they are the same as those in the FIM model.

3.5. The Very Anisotropic Rotation (VAR) Model

The VAR model proposed by Mason et al.[46] corresponds to the SRLS model wherein the internal motion is so strongly coupled to the cage that we can assume the orienting potential coefficient of $D^2_{00}(\Omega_{C'M})$ in eq 6 becomes extremely large (i.e. $c_0^2 \rightarrow \infty$). Also for simplicity one lets $R^c_{||} = R^c_\perp$. Then the overall

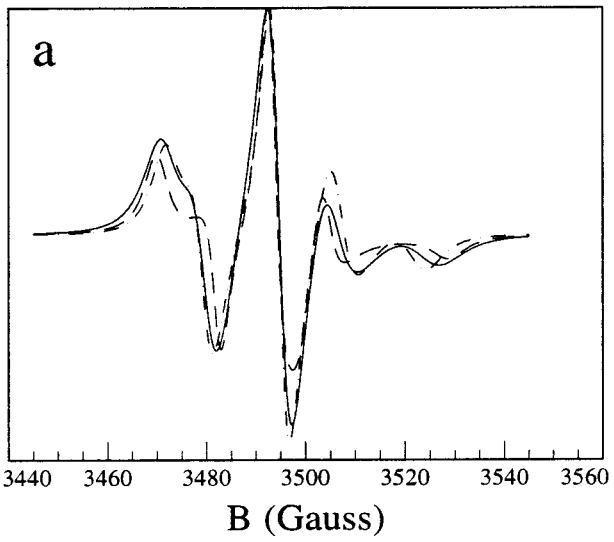

Figure 4. 9 GHz theoretical spectra: (a) Comparisons between SRLS (solid line), MOMD (dashed), and FIM (dotted line) models, using the parameters listed in Table 1. (b) NLLS fits of MOMD (dashed line) and FIM (dotted line) models to simulated SRLS spectra (solid line). The best fit parameters are given in Table 2.

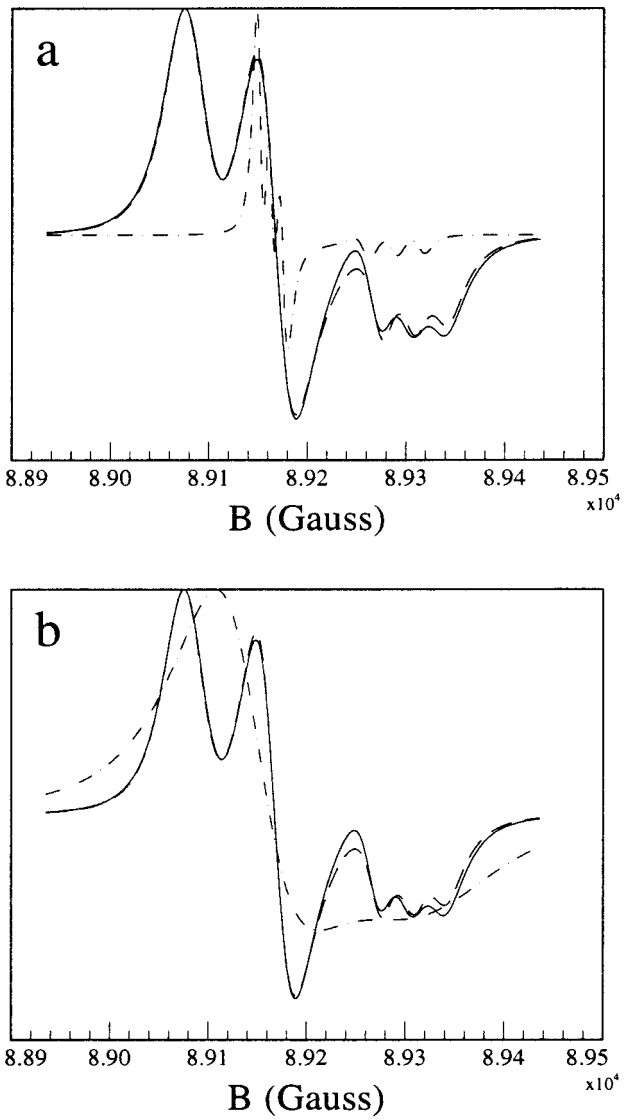

Figure 5. 250 GHz theoretical spectra: (a) Comparisons between SRLS (solid line), MOMD (dashed) and FIM (dotted line) models, using the parameters listed in Table 1. (b) NLLS fits of MOMD (dashed line) and FIM (dotted line) models to simulated SRLS spectra (solid line). The best fit parameters are given in Table 3.

TABLE 1: Magnetic Tensor Parameters

	xx	*yy*	*zz*
g	2.0096	2.0067	2.0028
A (gauss)	7.47	7.21	36.3
f_0 (GHz)[a]	9.786	94.696	249.721
B_0 (gauss)[b]	3495	33820	89186

[a] f_0 gives the exact values of the resonance frequency that is nominally given as 9, 95, or 250 GHz. [b] B_0 corresponds to the center field ($g = 2.002\,31$) for the respective Larmor frequencies.

TABLE 2: MOMD and FIM Fitting Parameters to a SRLS Simulated 9 GHz Spectrum

model	$R_\perp^c = R_\parallel^c \times 10^{-7}$ (s^{-1})	$R_\perp^o = R_\parallel^o \times 10^{-8}$ (s^{-1})	c_0^2	S_0^2	W_1 (G)
SRLS	1	1	3	(0.61)	2
MOMD		0.53	1.6	(0.36)	1.4
FIM	2.6			0.89	1.1

TABLE 3: MOMD and FIM Fitting Parameters to a SRLS Simulated 250 GHz Spectrum

model	$R_\perp^c = R_\parallel^c \times 10^{-7}$ (s^{-1})	$R_\perp^o = R_\parallel^o \times 10^{-8}$ (s^{-1})	c_0^2	S_0^2	W_1 (G)
SRLS	1	1	3	(0.61)	2
MOMD		0.99	2.83	(0.58)	1.9
FIM	16.3			1.0	54.8

diffusion operator of eq 2 takes on the following simple form:

$$\hat{\Gamma} = \hat{\Gamma}^{\text{internal}} = R_\parallel^o \hat{\mathbf{J}}_z^{o2} + R_\perp^c \hat{\mathbf{J}}^{o2} \tag{20}$$

Also, in this case the form of the spin Hamiltonian given by eq 1 is used directly. Here, only the diffusion parameters $R_\parallel^o$ and $R_\perp^c$ and the tilt angle β_{MG} are needed, when only β_{MG} is sufficient to determine Ω_{MG}.

The base disk model used by Keyes et al.[47] is a simple variant of the VAR model. It considers the spin-labeled base as the diffusion system rather than the DNA helix. The principal diffusion axis coincides with the bond connecting the spin label to the base and tilts from the magnetic principal axis by a static angle. The model treats the diffusion process as an anisotropic body rotating in an isotropic environment. The two diffusion rates represent all motions contributing to the motion of the labeled base including the global tumbling. $R_\perp^c$ in eq 21

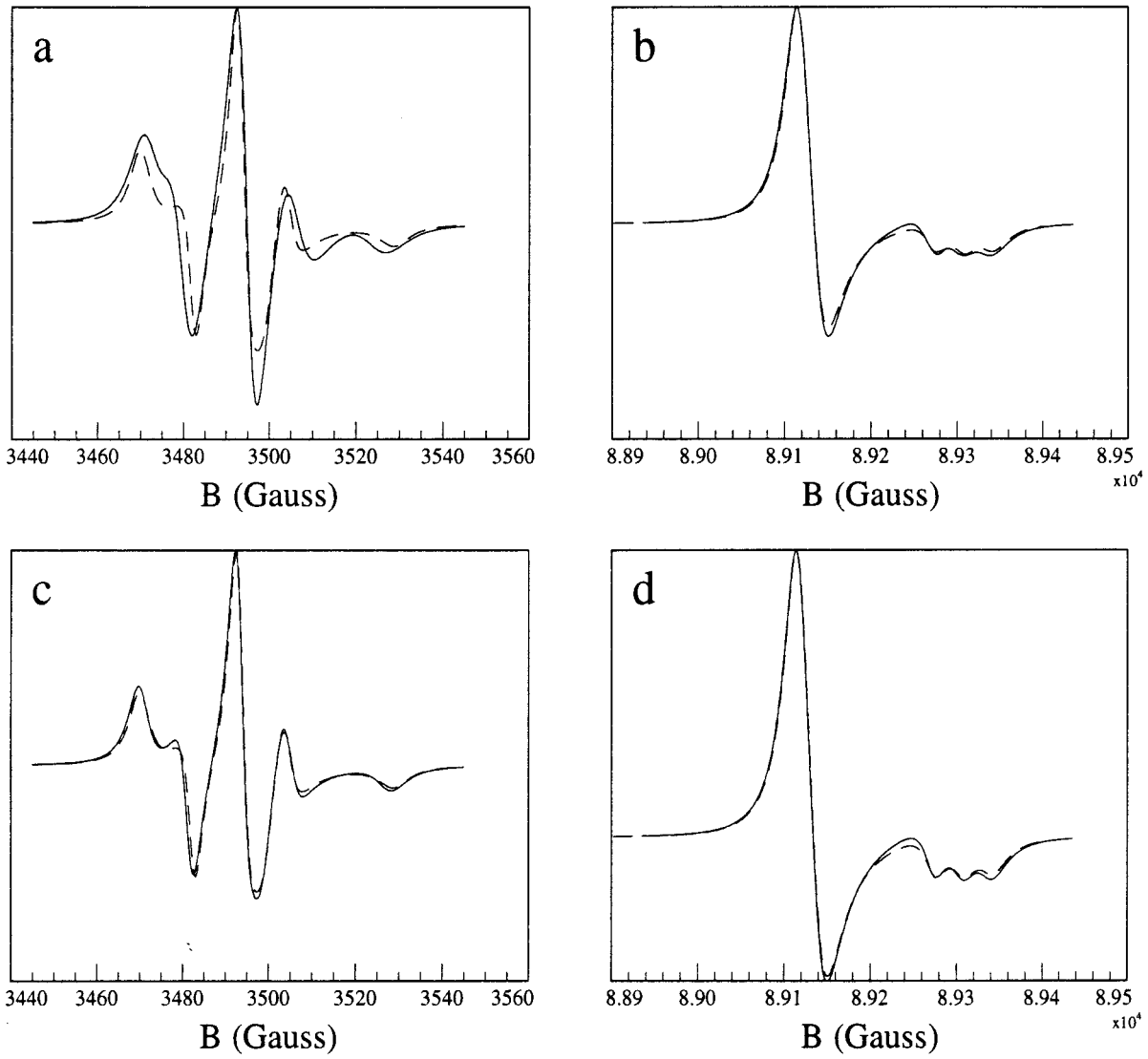

Figure 6. Comparison between SRLS (solid) and MOMD (dashed) models. $c_0^2 = 3$, $W = 2$ G, $\beta_{CC'} = 0$, $R_\perp^o = 1 \times 10^8$ s^{-1}, $R_\parallel^o = 1 \times 10^9$ s^{-1}. The other parameters are (a) 9 GHz: $R_\perp^c = 1 \times 10^7$ s^{-1}, $R_\parallel^c = 5 \times 10^7$ s^{-1}. (b) 250 GHz: parameters are the same as those in (a). (c) 9 GHz: $R_\perp^c = 1 \times 10^6$ s^{-1}, $R_\parallel^c = 5 \times 10^6$ s^{-1}. (d) 250 GHz: parameters are the same as those in (c).

includes the effect of all motions, except for the internal motion of the N−O bond, which is given by $R_\parallel^o$.

4. Theoretical Simulations

We have described the SRLS model and a few simplified models derived from it in different motional limits. These limiting models contain fewer model parameters and thus require less experimental "resolution" to extract dynamic and structural information about the systems under investigation. However, certain limiting criteria must be fulfilled for these simplified models to yield reliable information. In this section, we will compare the various models presented in this work and consider the consequences of an improper use of the limiting models. The precise frequencies and their associated center magnetic fields (for $g = 2.00231$) as well as the magnetic tensor components used in this section are listed in Table 1.

Let us first provide a "test" of the effects of utilizing an oversimplified model. That is, we shall assume that a SRLS model is the correct one and utilize some spectra simulated with the SRLS model as the reference. We shall then attempt to obtain best fits (in a least squares sense) to these spectra using the two simpler models: MOMD and FIM. We shall attempt to see if a limiting model might be satisfactory. By comparing results obtained at a low frequency (9 GHz) with those obtained at a high frequency (250 GHz), we wish to see to what extent the simultaneous use of these two frequencies can resolve ambiguities and inaccuracies that would exist if only a single frequency were used.

In Figure 4a, we compare the theoretical 9 GHz ESR spectra of the SRLS, MOMD, and FIM models, using the following parameters: $R_\perp^o = R_\parallel^o = 10^8$ s^{-1}, $R_\perp^c = R_\parallel^c = 10^7$ s^{-1}, $c_0^2 = 3$ ($S_0^2 = 0.605$), $\beta_{CC'} = 0$, $\beta_{MG} = 0$, and a Lorentzian line width $W = 2$ G. This corresponds to a case in which the internal rotations are fairly (but not very) fast, the overall motion is an order of magnitude slower, and there is substantial internal ordering. It can be seen from the figure that, for the given set of parameters, the FIM model, while it does not give a very good fit, does gives a better approximation to the SRLS model than does the MOMD model.

We now perform two nonlinear least-squares (NLLS) fits to the SRLS spectrum with the MOMD and FIM models respectively, as though they were each the correct model. As Figure 4b indicates, reasonable, but not perfect, fits are obtained in both cases, but with the high field line being better reproduced

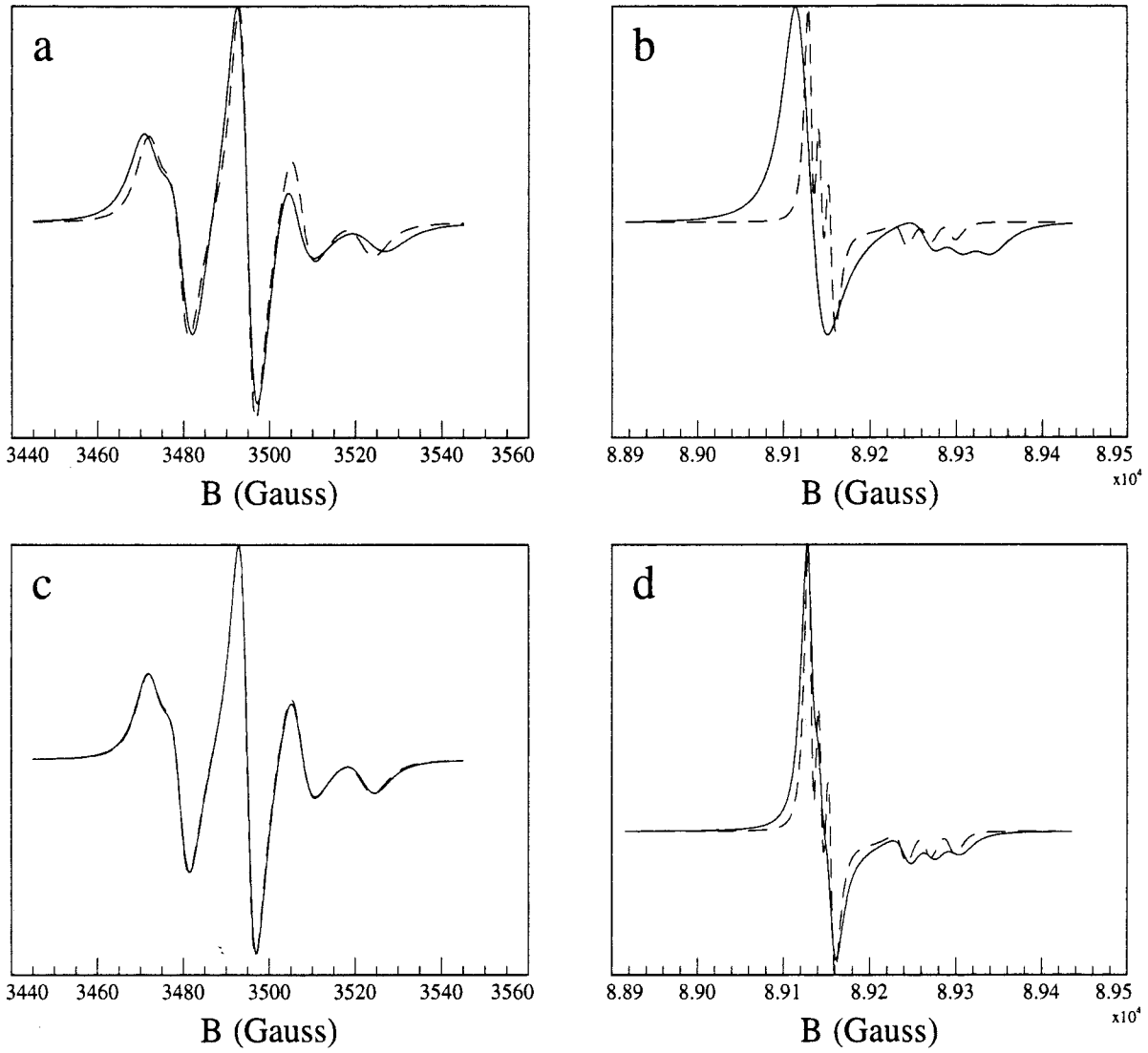

Figure 7. Comparison between SRLS (solid) and FIM (dashed) models. $c_0^2 = 3$, $W = 2$ G, $\beta_{CC'} = 0$, $R_\perp^c = 1 \times 10^7$ s^{-1}, $R_\parallel^c = 1 \times 10^8$ s^{-1}. The other parameters are (a) 9 GHz: $R_\perp^o = 1 \times 10^8$ s^{-1}, $R_\parallel^o = 1 \times 10^9$ s^{-1}. (b) 250 GHz: parameters are the same as those in (a). (c) 9 GHz: $R_\perp^o = 1 \times 10^9$ s^{-1}, $R_\parallel^o = 1 \times 10^{10}$ s^{-1}. (d) 250 GHz: parameters are the same as those in (c).

by the FIM model and the low field line better represented by the MOMD model. The best fit parameters are listed in Table 2. We find the following: (i) The FIM model overestimates the order parameter and underestimates the size of a DNA or protein complex (i.e., its R^c is too large). Since the internal motion is assumed to be in the fast limit, the FIM model with the correct parameters produces narrowed lines, as shown in Figure 4a. This is compensated for by reducing the effect of the fast averaging in the only way that the FIM model is capable of, i.e., by increasing the order parameter from 0.61 to 0.89. In addition, is was necessary to increase the global tumbling rate somewhat. (Note that we constrained $R_\perp^c = R_\parallel^c$ for simplicity). (ii) By contrast, the MOMD model predicts a lower ordering and a slower internal dynamics than the correct values. This is due to the extremely slow global motion assumed in the MOMD model, which tends to make the line shapes more like the rigid limit, compared with the SRLS spectrum where the global motional rate is 10^7 s^{-1} (Figure 4a). To fit the SRLS spectrum, the order parameter has been reduced from 0.61 to 0.36 by the MOMD model. This reduces the effect of the rigid-limit assumption for the global motion. The internal dynamics has been slowed down by a factor of about 2, since it must partly compensate for the global motion that was not included.

A similar comparison is also made between SRLS, MOMD and FIM models at 250 GHz, with the corresponding model parameters given in Table 3. As displayed in Figure 5a, the spectra from SRLS and MOMD models using the same parameters show good agreement except in the high field region, but the FIM model provides a very poor fit. This is just the opposite of the situation for 9 GHz. A NLLS fit to the SRLS spectrum using the MOMD model did not significantly improve the agreement between the spectra from the two models (Figure 5b and Table 3). This result indicates that a global motion of 10^7 s^{-1} is already in the rigid limit with respect to the 250 GHz ESR time scale. On the other hand, the FIM model gives a spectrum, which is so different from that from the SRLS model that it even failed to reproduce the SRLS spectrum in a NLLS fit (cf. Figure 5b and Table 2). In other words, for motional rates relevant to DNA or protein systems, the SRLS model can be well represented by the simpler MOMD model at 250 GHz. In the recent study on spin label lysozyme,[7] this feature was utilized in order to effectively separate the motions of different

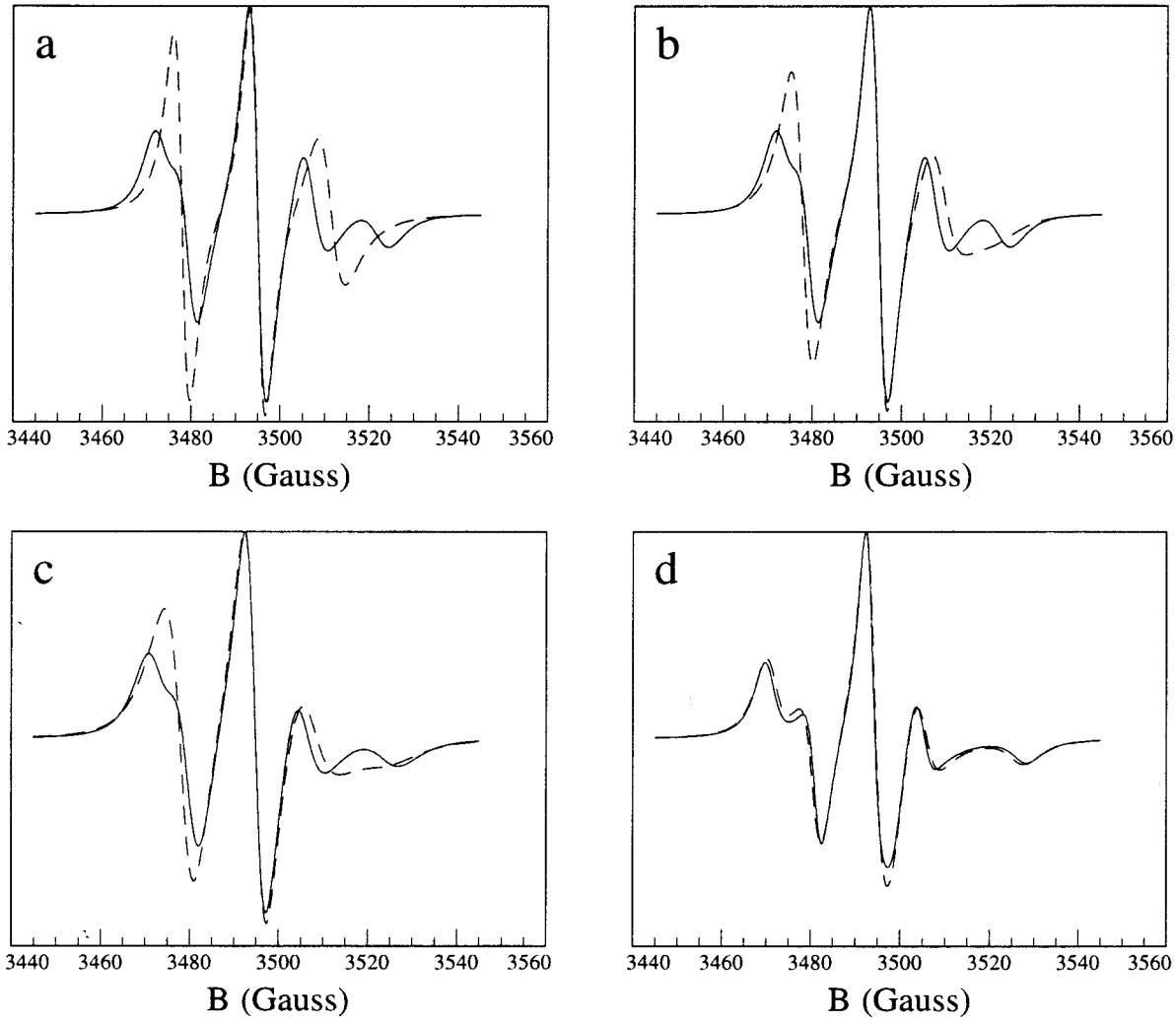

Figure 8. 9 GHz SRLS model simulations (solid, $\beta_{CC'} = 0$; dashed, $\beta_{CC'} = 90$). $c_0^2 = 3$, $W = 2$ G. The other parameters are (a) $R_\perp^c = 1 \times 10^7$ s^{-1}, $R_\parallel^c = 1 \times 10^8$ s^{-1}, $R_\perp^o = 5 \times 10^9$ s^{-1}, $R_\parallel^o = 1 \times 10^{10}$ s^{-1}. (b) $R_\perp^c = 1 \times 10^7$ s^{-1}, $R_\parallel^c = 5 \times 10^7$ s^{-1}, $R_\perp^o = 5 \times 10^9$ s^{-1}, $R_\parallel^o = 1 \times 10^{10}$ s^{-1}. (c) $R_\perp^c = 1 \times 10^7$ s^{-1}, $R_\parallel^c = 1 \times 10^8$ s^{-1}, $R_\perp^o = 1 \times 10^8$ s^{-1}, $R_\parallel^o = 1 \times 10^9$ s^{-1}. (d) $R_\perp^c = 1 \times 10^6$ s^{-1}, $R_\parallel^c = 5 \times 10^6$ s^{-1}, $R_\perp^o = 1 \times 10^8$ s^{-1}, $R_\parallel^o = 1 \times 10^9$ s^{-1}.

time scales. That is, from MOMD fits to the 250 GHz experimental spectra, reliable parameters were produced for the internal motions. Then these internal motional parameters were employed in a full SRLS model fit to the 9 GHz spectra to yield the global tumbling rate.

More generally, we see that the high frequency spectra provide better sensitivity to the faster motions (e.g., the internal motion), whereas in the low frequency spectra they are nearly averaged out, but these latter spectra then provide the greater sensitivities to the slow motions (e.g., the global tumbling motion). Given the limited resolution of the EPR spectra, they allow for ambiguity in the fitting model (especially at low frequency, cf. Figure 4b). However this example implies that, when fit simultaneously, low frequency and high frequency spectra can provide the information needed to fit a model as complex as the SRLS model.

We next wish to estimate the dynamic range over which the MOMD result is a good approximation to the SRLS result for both 9 and 250 GHz. This is shown in Figure 6 where we compare MOMD results to SRLS results using the same parameters. We see from Figure 6c, for the case of 9 GHz ESR, that when $R_\perp^c$ and $R_\parallel^c$ are 1 and 5×10^6 s^{-1}, respectively, the motion has already slowed down sufficiently that the SRLS result is roughly approximated by the MOMD result; however for $R_\perp^c$ and $R_\parallel^c$ appreciably greater than this (e.g., 1 and 5×10^7 s^{-1} respectively, cf. Figure 6a), then MOMD is a very poor approximation to SRLS. However, for 250 GHz the MOMD limit is a reasonable approximation even with substantial global motion (cf. Figure 6b and Figure 5a).

In Figure 7, we have an analogous comparison between the FIM result and the SRLS result. Here we compare results for a range of large values of $R_\perp^o$ and $R_\parallel^o$ to see when the FIM model approximates the SRLS result. In Figure 7a and b, we use values of 0.1 and 1×10^9 s^{-1} respectively, which are already quite fast. Neither the 9 GHz nor the 250 GHz spectra show satisfactory agreement. The FIM model is not an acceptable approximation in either case. However, when $R_\perp^o$ and $R_\parallel^o$ are both increased by 1 order of magnitude, the 9 GHz SRLS spectrum (cf. Figure 7c) is very well approximated by the FIM model (see also Figure 4a for somewhat different values), although for 250 GHz (cf. Figure 7d) SRLS is poorly approximated by the FIM model. One must increase $R_\perp^o$ and $R_\parallel^o$ by additional order of magnitude for the FIM model to yield a rough approximation to the corresponding 250 GHz SRLS spectrum (not shown).

In addition, by comparison of Figures 6 and 7, in which anisotropic (but axially symmetric) diffusion has been intro-

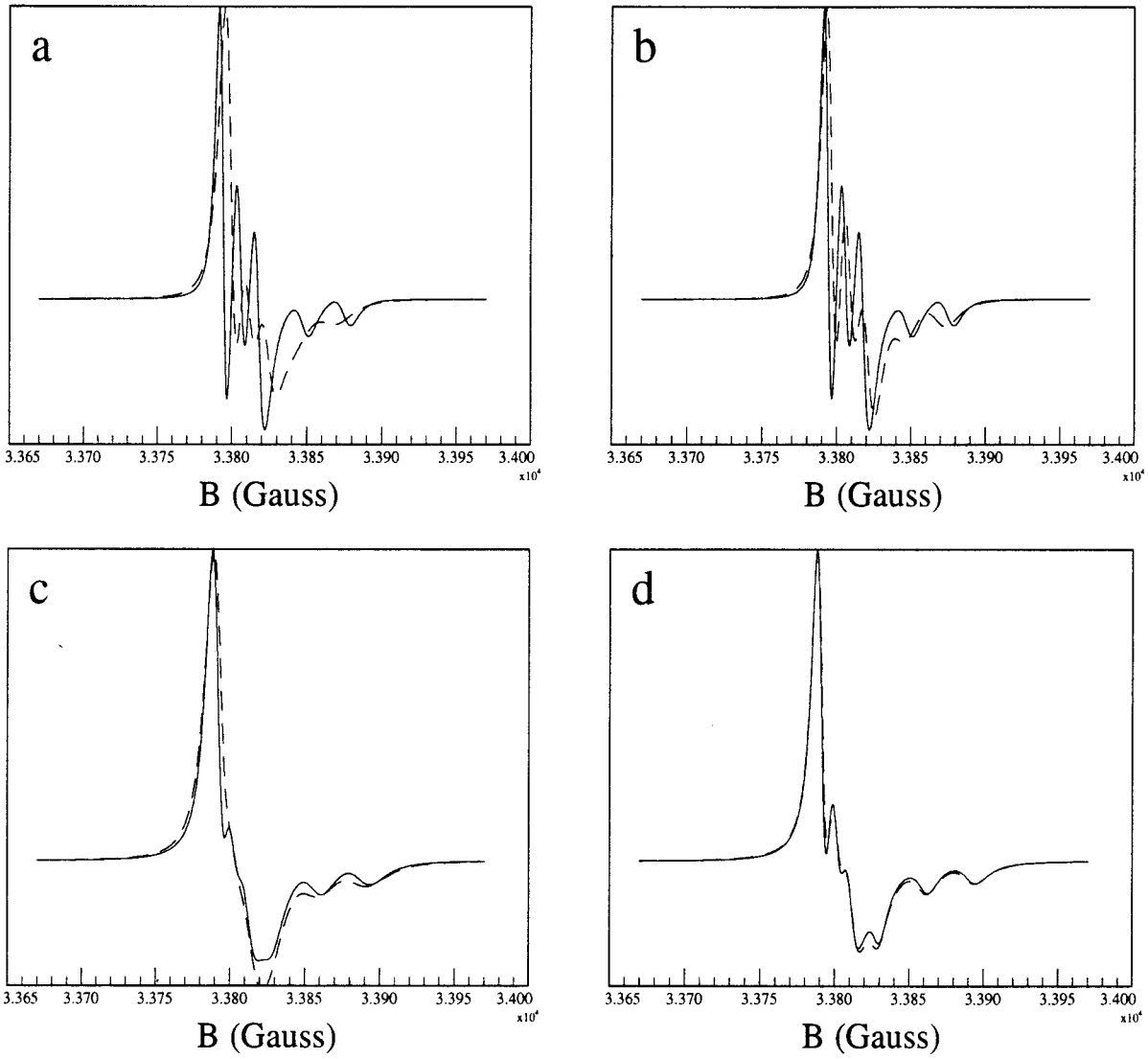

Figure 9. 95 GHz SRLS model simulations (solid: $\beta_{CC'} = 0$; dashed, $\beta_{CC'} = 90$). The parameters are the same as in Figure 8.

duced, with Figures 4a and 5a for isotropic diffusion, we can note the sensitivity to anisotropy in diffusion. First, a comparison of Figure 6a with Figure 4a shows just a small change in both the predicted 9 GHz SRLS and MOMD spectra by increasing $N^{c} \equiv R_{||}^{c}/R_{\perp}^{c}$ from 1 (Figure 4a) to 5 (Figure 6a) and $N^{o} \equiv R_{||}^{o}/R_{\perp}^{o}$ from 1 to 10. On the other hand, a comparison of Figure 6b with Figure 5a shows a much more substantial spectral change at 250 GHz for the same change in N^{c} and N^{o}. Since Figure 6b is already close to the MOMD limit, we may safely conclude that this is mainly due to the increase in $R_{||}^{o}$ that yielded $N^{c} = 5$. This indicates that the 250 GHz spectra will be more sensitive to anisotropy in the internal dynamics than the 9 GHz spectra. In addition, a comparison of the SRLS spectra in Figures 6a and 7a for 9 GHz vs. Figures 6b and 7b for 250 GHz shows that when N^{c} increases from 5 to 10, there is a noticeable change in the 9 GHz spectrum, but the 250 GHz spectrum is virtually unchanged. This indicates that the 9 GHz spectra will be more sensitive to anisotropy in the overall motional dynamics. This is, of course the expected result, since the 250 GHz spectra are, in general, insensitive to all aspects of the overall motional dynamics.

We now introduce a cage tilt $\beta_{CC'}$ into the SRLS model and address the issue of the ability to distinguish $\beta_{CC'}$. We do this for the three frequencies: 9, 95, and 250 GHz. In Figure 8 we show the results for 9 GHz. Case a is for $R_{\perp}^{c} = 1 \times 10^{7}$ s^{-1}, $R_{||}^{c} = 1 \times 10^{8}$ s^{-1}, $R_{\perp}^{o} = 5 \times 10^{9}$ s^{-1}, $R_{||}^{o} = 1 \times 10^{10}$ s^{-1}, i.e., rather fast motions. In case b, $R_{||}^{c}$ drops by a factor of 2 from case a to 5×10^{7} s^{-1}. In case c $R_{\perp}^{o}$ and $R_{||}^{o}$ drop by factors of 50 and 10, respectively, from case a to $R_{\perp}^{o} = 1 \times 10^{8}$ s^{-1} and $R_{||}^{o} = 1 \times 10^{9}$ s^{-1}, whereas in case d $R_{\perp}^{c}$ and $R_{||}^{c}$ drop by factors of 10 and 20 respectively from case a to $R_{\perp}^{c} = 1 \times 10^{6}$ s^{-1} and $R_{||}^{c} = 5 \times 10^{6}$ s^{-1}. In case a we observe significant differences between the $\beta_{CC'} = 90°$ and 0° cases. In case b, the modest drop in $R_{||}^{c}$ reduces these differences somewhat, undoubtedly because the ratio $R_{||}^{c}/R_{\perp}^{c}$ is reduced [recall that, as $R_{||}^{c}/R_{\perp}^{c}$ approaches one, i.e., isotropic global tumbling, cage tilt should have no effect on the spectrum]. Note, however, from case c that a large drop in $R_{||}^{o}$ and $R_{\perp}^{o}$ also tends to reduce the effect of $\beta_{CC'}$. When both $R_{||}^{c}$ and $R_{\perp}^{c}$ become very small, i.e., case d, then SRLS is approaching the MOMD limit, wherein the spectrum must become independent of $\beta_{CC'}$, as confirmed in Figure 8d.

In Figure 9 for 95 GHz and 10 for 250 GHz we see the same cases a−d illustrated. When we compare the respective case a's, we observe substantial differences between $\beta_{CC'} = 0°$ and 90° for all frequencies, but they are somewhat reduced at 250 GHz. We attribute this to the fact that the high frequency

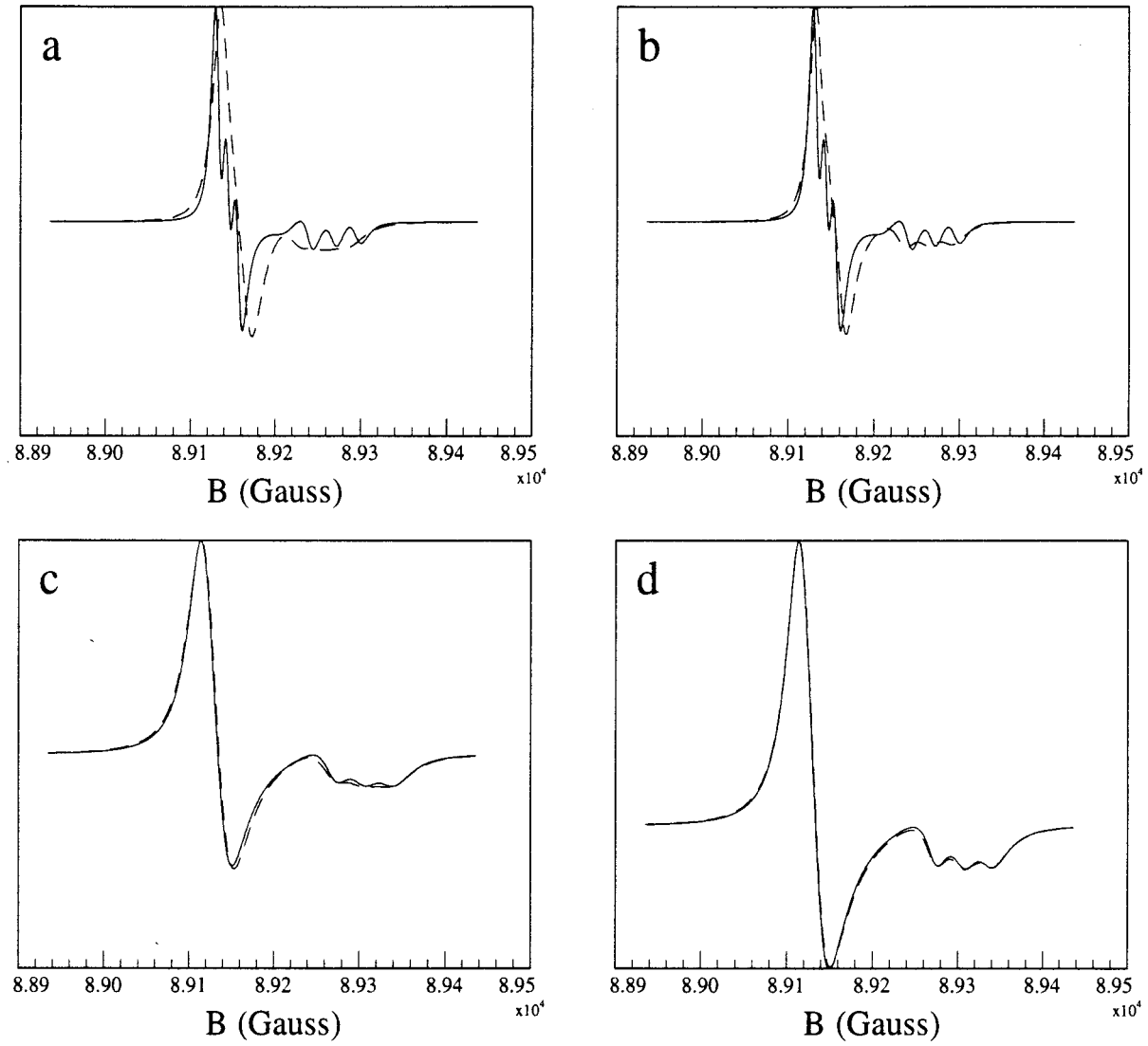

Figure 10. 250 GHz SRLS model simulations (solid, $\beta_{CC'} = 0$; dashed, $\beta_{CC'} = 90$). The parameters are the same as those in Figure 8.

spectrum at 250 GHz is closer to the MOMD limit, which suppresses sensitivity to $\beta_{CC'}$, as we have seen. This reduced resolution to $\beta_{CC'}$ at the high frequencies is seen for the case b series where the $R_{||}^c/R_{\perp}^c$ anisotropy ratio is reduced by a factor of 2. However, the large reductions in $R_{||}^o$ and $R_{\perp}^o$ also suppress the sensitivity to $\beta_{CC'}$, especially at the higher frequencies. Finally, the MOMD limit is reached at all frequencies for case d. Clearly, a sensitivity to $\beta_{CC'}$ requires first and foremost that $R_{||}^c/R_{\perp}^c \neq 1$, but also that the spectrum not be near the MOMD limit, and this is made more probable by using low frequencies. In addition, slow internal motions also appear to mask this sensitivity, as the spectrum approaches the rigid limit. Actually, one does not have to be very close to the rigid limit for the loss of sensitivity to $\beta_{CC'}$. In fact, if one decreases the values of $R_{\perp}^o$ and $R_{||}^o$ from those for case d, each by a factor of 10, the spectra are still not close the rigid-limit (cf. Figure 11). Thus, the best way to enhance sensitivity to $\beta_{CC'}$ would be to increase the temperature to produce faster motional rates in general.

The SRLS and the related simplified models presented in this work have been applied to a protein system[7] and some DNA systems.[8] For the protein system (T4 lysozyme), since the overall rotational diffusion rate was found to be too slow to significantly affect the 250 GHz ESR spectra ($R_{\perp}^c \approx R_{||}^c \approx 1 \times 10^7$ s^{-1}), the MOMD model was employed to analyze the 250 GHz data to yield dynamical information for the internal motion [$R_{\perp}^o \approx (2-4) \times 10^8$ s^{-1}, $R_{||}^o \approx 10^7-10^8$ s^{-1} and $c_0^2 \sim 4$ and 1.5 for different species]. However, in the slower "time scale" of the 9 GHz ESR experiment, the overall rotational diffusion had to be accounted for in the spectral analysis as noted above. This was accomplished by using the SRLS model. In this way a simultaneous fit was successfully obtained for both 9 GHz and 250 GHz ESR spectra. For the DNA systems, since the 250 GHz ESR data was not available, a different approach was adopted. The overall diffusional rates were determined using the hydrodynamic theory and fixed in the 9 GHz ESR spectral analysis. Since the overall tumbling is both anisotropic and in the slow motional regime with respect to the 9 GHz ESR time scale [$R_{\perp}^c \approx (0.1-1.5) \times 10^7$ s^{-1}, $R_{||}^c \approx (0.1-3.6) \times 10^7$ s^{-1}], the anisotropic SRLS model with the cage tilt $\beta_{CC'}$ had to be used to obtain reliable internal dynamics [$R_{\perp}^o \approx 10^6-10^8$ s^{-1}, $R_{||}^o \approx 10^8-10^{10}$ s^{-1} and $c_0^2 \sim 0.8-3.0$, $\beta_{CC'} \approx 90$].

5. Summary and Comments

By means of spectral simulations of nitroxide spin label spectra at low and high frequencies, we have confirmed the fact that ESR at high frequencies will be more sensitive to the faster dynamics that may well be averaged out at lower frequencies,

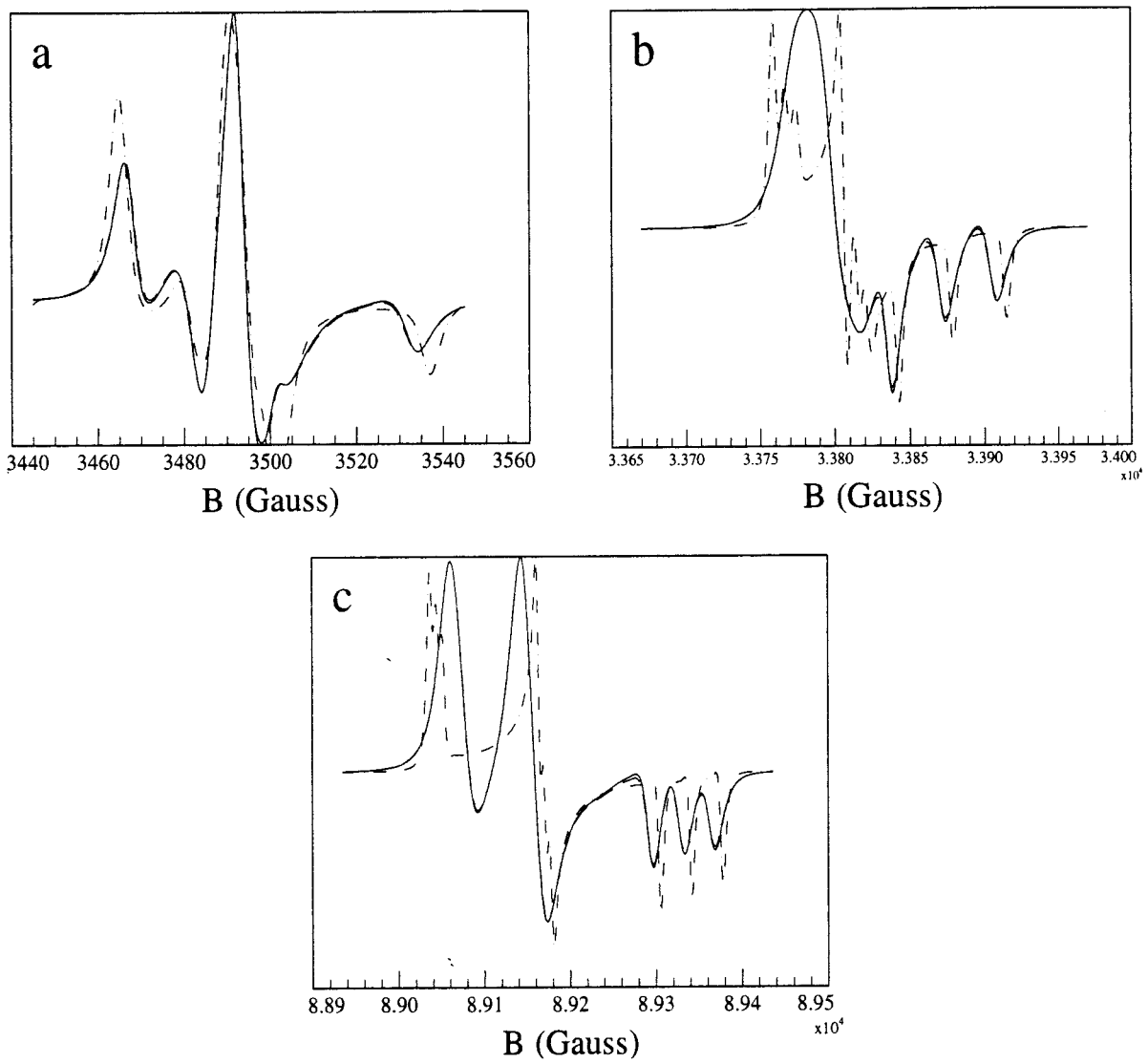

Figure 11. Comparison between SRLS (solid, $\beta_{CC'} = 0$; dashed $\beta_{CC'} = 90$; note that they are nearly identical) and rigid limit (dotted) models. $c_0^2 = 3$, $W = 2$ G, $R_\perp^o = 1 \times 10^7$ s^{-1}, $R_\parallel^o = 1 \times 10^8$ s^{-1}, $R_\perp^c = 1 \times 10^6$ s^{-1}, $R_\parallel^c = 5 \times 10^6$ s^{-1}. (a) 9 GHz, (b) 95 GHz, (c) 250 GHz.

whereas ESR at lower frequencies will be more sensitive to the slower dynamics that may well be frozen out at higher frequencies. A multifrequency study thus has the advantage of enabling one to decompose the dynamic modes into respective components acting on different time scales. In addition, examples were provided to show how individual spectra may be fit to oversimplified models due to their limited resolution to the dynamics, but this ambiguity can be removed by simultaneously utilizing spectra at different frequencies. Nevertheless, under certain limiting conditions, more general models such as the SRLS (or dynamic cage) model studied in this work will legitimately reduce to simpler models with fewer parameters, e.g., when the overall tumbling of the macromolecule is very slow, the MOMD model becomes satisfactory, especially for high frequency ESR spectra, and when the internal modes of motion are very fast, then the FIM model becomes satisfactory, especially for low frequency ESR spectra. While these limits may be useful for fitting individual ESR spectra, they in no way reduce the need for a multifrequency ESR study to obtain all the relevant dynamic (e.g., the diffusion coefficients), ordering (e.g., ordering parameter) and orientational (e.g., $\beta_{CC'}$ and β_{MG}) parameters for the various relevant modes of motion.

In addition to the reasons described in the previous paragraph for a multifrequency approach, there are indeed many subtle aspects requiring it. One that we studied in detail in this work is a determination of the cage tilt angle $\beta_{CC'}$, associated with the internal motion, which is possible to accomplish only when $R_\parallel^c/R_\perp^c$ is sufficiently different from unity. One may use high frequency ESR to freeze out the global motion, as we have seen, in order to more clearly study the internal motions, but it will also remove any effects of $\beta_{CC'}$ on such spectra. Low frequency ESR would then be required to obtain this important parameter, which gives the orientation of the principal axis of internal motion relative to the principal axes of the biomolecule.

The analysis in the paper treated the internal modes of motion in a rather simple manner, i.e., by means of the parameters: $R_\parallel^o$, $R_\perp^o$, c_0^2, c_2^2, and $\beta_{CC'}$. Just as it was possible to decompose the fast internal modes from the slower global tumbling by virtue of their different time scales by utilizing a multi-frequency ESR approach, one may expect that by extending the models used and by employing a range of several ESR frequencies, it should be possible to decompose the internal modes of motion into components acting over sufficiently different time scales. In spin-label work, one wishes at the very least to separate the

internal motion of the spin-label from the internal modes characteristic of the biomolecule. One simple approach for dealing with this is to use a spinning diffusion coefficient $R_{\|}^{\text{int}}$ to represent this spin-label motion, with $R_{\perp}^{\text{o}}$ playing the role of the composite of the other internal modes. This model assumes that the spin-label motion and other modes of internal motions are decoupled from each other and can be treated as independent processes.[48] However, a further decomposition of the other internal modes would still be desirable.[49]

We have so far not considered the case of two-site jumps, in which the internal diffusion axis jumps between two nonequivalent sites, each site having different orientation. This model has been employed in NMR relaxation studies of DNA systems. If the exchange rate between the two sites is too slow compared with the ESR time scale, the ESR line shape would be a superposition of the contributions from the two sites. These sites may have different dynamics, which are described by different model parameters. The general case in which the exchange rate is fast enough to affect the ESR line shape is a complex one, especially in the slow motional regime. In principle, it would be necessary to write a separate SLE for each site, which would include the respective diffusion operator for each site, as well as an exchange term between them.

In conjuction with the ESR approach discussed in this paper, one would want to utilize structural models to infer how the projections of the "characteristic" internal modes affect the local motion of the labeled residue, and this needs to be studied as a function of the different labeled sites. Whereas this would be a complex and tedious challenge, it could well lead to a detailed mapping of the dynamic structure of the macromolecule.

Finally, we note that time domain ESR, such as 2D-FT-ESR, has the capacity to look directly at relaxation processes, and unlike cw-ESR can distinguish between homogeneous broadening, which reports on dynamics, and inhomogeneous broadening, which often reports on microscopic ordering. More powerful multifrequency ESR approaches should ultimately emanate from such technologies.

Acknowledgment. We acknowledge helpful discussions with Professors Wayne L. Hubbell and Albert M. Bobst and Drs. Jeff Barnes, David Schneider, and Keith Earle. This work was supported by grants from NIH and NSF. The computations were performed at the Cornell Theory Center.

References and Notes

(1) Berliner, L., Ed. *Spin Labeling: Theory and Applications;* Academic Press: New York, 1976.
(2) Hubbell, W. L.; Mchaourab, H. S.; Altenbach, C.; Lietzow, M. A. *Structure* **1996**, *4*, 779.
(3) Borbat, P. P.; Crepeau, R. H.; Freed, J. H. *J. Magn. Reson.* **1997**, *127*, 155.
(4) Sastry, V. S. S.; Polimeno, A.; Crepeau, R. H.; Freed, J. H. *J. Chem. Phys.* **1996**, *105*, 5753.
(5) Budil, D. E.; Earle, K. A.; Lynch, W. B.; Freed, J. H. In *Advanced EPR: Applications in Biology and Biochemistry*; Hoff, A. J., Ed.; Elsevier: Amsterdam, 1989; Chapter 8.
(6) Barnes, J. P.; Freed, J. H. *Rev. Sci. Instrum.* **1997**, *68*, 2838.
(7) Barnes, J. P.; Liang, Z.; Mchaourab, H. S.; Freed, J. H.; Hubbell W. L. *Biophys. J.* **1999**, *76*, 3298.
(8) Liang, Z.; Freed, J. H. Manuscript in preparation.
(9) Kay, L. E. *Nature, Structural Biology, NMR Supplement* **1998**, July, 513.
(10) Peng, J. W.; Wagner, G. *Methods Enzymol.* **1994**, *239*, 563.
(11) Hartmann, B.; Lavery, R. *Q. Rev. Biophys.* **1996**, *29*, 309.
(12) Keyes, R. S.; Bobst, A. M. In *Biological Magnetic Resonance, Volume 14: The Next Millennium*; Berliner, L., Ed.; Plenum Press: New York, 1998; Chapter 7.
(13) Lipari, G.; Szabo, A. *Biochemistry* **1981**, *20*, 6250.
(14) Lipari, G.; Szabo, A. *J. Am. Chem. Soc.* **1982**, *104*, 4546.
(15) Lipari, G.; Szabo, A. *J. Am. Chem. Soc.* **1982**, *104*, 4559.
(16) Hubbell, W. L.; Altenbach, C. *Curr. Opin. in Struct. Biol.* **1994**, *4*, 566.
(17) Steinhoff, H.-J.; Mollaaghababa, R.; Altenbach, C.; Khorana, H. G.; Hubbell, W. L. *Biophys. Chem.* **1995**, *56*, 89.
(18) Mchaourab, H. S.; Lietzow, M. A.; Hideg, K.; Hubbell, W. L. *Biochemistry* **1996**, *35*, 7692.
(19) Mchaourab, H. S.; Oh, K. J.; Fang, C. J.; Hubbell, W. L. *Biochemistry* **1997**, *36*, 307.
(20) Artyukh, R. I.; Kachalova, G. S.; Samaryanov, B. A.; Timofeev, V. P. *Mol. Biol.* **1995**, *29*, 87.
(21) Kao, S.-C.; Polnaszek, C. F.; Toppin, C. R.; Bobst, A. M. *Biochemistry* **1983**, *22*, 5563.
(22) Spaltenstein, A.; Robinson, B. H.; Hopkins, P. B. *Biochemistry* **1989**, *28*, 9484.
(23) Hustedt, E. J.; Kirchner, J. J.; Spaltenstein, A.; Hopkins, P. B.; Robinson, B. H. *Biochemistry* **1995**, *34*, 4369.
(24) Bobst, E. V.; Keyes, R. S.; Cao, Y. Y.; Bobst, A. M. *Biochemistry* **1996**, *35*, 9309.
(25) Keyes, R. S.; Bobst, E. V.; Chao, Y. Y.; Bobst, A. M. *Biophys. J.* **1997**, *72*, 282.
(26) Ernst, R. R.; Bodenhausen, G.; Wokaun, A. *Principles of Nuclear Magnetic Resonance in One and Two Dimensions*; Oxford: New York, 1987.
(27) Freed, J. H.; Bruno, G. V.; Polnaszek, C. F. *J. Phys. Chem.* **1971**, *55*, 5270.
(28) Polnaszek, C. F.; Bruno, G. V.; Freed, J. H. *J. Chem. Phys.* **1973**, *58*, 3185.
(29) Freed, J. H. In *Spin Labeling: Theory and Applications;* Berliner, L., Ed.; Academic Press: New York, 1976; p 53.
(30) Schneider, D. J.; Freed, J. H. In *Biological Magnetic Resonance*; Berliner, L. J., Reuben, J., Ed.; Plenum Publishing Corporation: New York, 1989; Vol. 8.
(31) Schneider, D. J.; Freed, J. H. *Adv. Chem. Phys.* **1989**, *73*, 387.
(32) Earle, K. A.; Budil, D. E.; Freed, J. H. *J. Phys. Chem.* **1993**, *97*, 13289.
(33) Polimeno, A.; Freed, J. H. *J. Phys. Chem.* **1995**, *99*, 10995.
(34) Polnaszek, C. F.; Freed, J. H. *J. Phys. Chem.* **1975**, *79*, 2283.
(35) Freed, J. H. *J. Chem. Phys.* **1977**, *66*, 4183.
(36) Campbell, R. F.; Meirovitch, M.; Freed, J. H. *J. Phys. Chem.* **1979**, *83*, 525.
(37) Earle, K. A.; Moscicki, J. K.; Polimeno, A.; Freed, J. H. *J. Chem. Phys.* **1997**, *106*, 9996.
(38) Polimeno, A.; Freed, J. H. *Adv. Chem. Phys.* **1993**, *83*, 89.
(39) Hustedt, E. J.; Spaltenstein, A.; Kirchner, J. J.; Hopkins, P. B.; Robinson, B. H. *Biochemistry* **1993**, 32, 1774.
(40) Timofeev, V. P.; Samarianov, B. A. *Appl. Magn. Reson.* **1993**, *4*, 523.
(41) Meirovitch, E.; Nayeem, A.; Freed, J. H. *J. Phys. Chem.* **1984**, *88*, 3454.
(42) Budil, D. B.; Lee, S.; Saxena, S.; Freed, J. H. *J. Magn. Reson.* **1996**, *120*, 155.
(43) Hubbell, W. L.; McConnell, H. M. *J. Am. Chem. Soc.* **1971**, *93*, 314.
(44) McFarland, B. G.; McConnell, H. M. *Proc. Nat. Acad. Sci. U.S.A.* **1971**, *68*, 1274.
(45) Tirado, M. M.; de la Torre, J. G. *J. Chem. Phys.* **1980**, *73*, 1986.
(46) Mason, R. P.; Polnaszek, C. F.; Freed, J. H. *J. Phys. Chem.* **1974**, *78*, 1324.
(47) Keyes, R. S.; Bobst, A. M. *Biochemistry* **1995**, *34*, 9265.
(48) In the special case when the axis of spin-label diffusion is coincident with the effective symmetry axis of the other modes of internal motions, or if $R_{\|}^{\text{o}} = R_{\perp}^{\text{o}}$, then $\hat{\Gamma}^{\text{internal}}$ simplifies to[36] $\hat{\Gamma}^{\text{internal}} = R_{\|}^{\text{int}}\hat{\mathbf{J}}_z^{\text{o}2} + [R_{\perp}^{\text{o}}\hat{\mathbf{J}}^{\text{o}2} + (R_{\|}^{\text{o}} - R_{\perp}^{\text{o}})\hat{\mathbf{J}}_z^{\text{o}2}]$.
(49) In the spirit of the present SRLS model we can illustrate how one may begin to accomplish this. That is, one can try to employ a fast internal motional limit for the nitroxide internal motion for the low frequency ESR spectra. After averaging over this motion, then the full SRLS model may be employed to yield both $R_{\perp}^{\text{o}}$ and $R_{\|}^{\text{o}}$ for the "characteristic" internal modes, assumed to be slower. The analysis of the high frequency ESR spectra on the same system could be simplified if the global motion is slow enough to have been frozen out. One must then perform a MOMD-like averaging over all orientations of the macromolecule, but the SRLS model could still be used such that $R_{\perp}^{\text{c}}$ and $R_{\|}^{\text{c}}$ of the SRLS model now represent the "characteristic" internal modes, whereas $R_{\perp}^{\text{o}}$ and $R_{\|}^{\text{o}}$ represent the internal nitroxide motion. Despite the different usages of the SRLS model for the low and high frequency spectra, these spectra could still be simultaneously analyzed to provide a decomposition in terms of three time scales. One would, of course, be advised to use more than one high frequency and low frequency ESR spectrum. In this spirit, generalizations to more complex cases may be readily conceived.